Magnetization Reversal in Ferromagnetic Films Patterned with Antiferromagnetic Gratings of Various Sizes

Magnetization Reversal in Ferromagnetic Films Patterned with Antiferromagnetic Gratings of Various Sizes

F. Liu and C. A. Ross*

Department of Materials Science and Engineering, Massachusetts Institute of Technology, 77 Massachusetts Avenue, Cambridge, Massachusetts 02139, USA

(Received 6 July 2015; revised manuscript received 12 October 2015; published 18 November 2015)

The magnetic switching behavior in continuous NiFe films patterned with IrMn gratings is investigated experimentally and with micromagnetic simulations. The samples made by a two-step deposition process consist of a 10-nm-thick NiFe layer on which is placed 10-nm-thick IrMn stripes with width from 100 to 500 nm and period from 240 nm to 1 μm. Exchange bias is introduced by field cooling in directions parallel or perpendicular to the IrMn stripes. The samples display a two-step hysteresis loop for higher stripe width and period, as the pinned and unpinned regions of the NiFe reverse independently but a one-step loop for lower stripe periods. The transition between these regimes is reproduced by micromagnetic modeling.

DOI: 10.1103/PhysRevApplied.4.054005

I. INTRODUCTION

Exchange bias between a ferromagnet (FM) and an antiferromagnet (AFM) is important in understanding magnetic exchange and its applications in devices such as magnetic random-access memories and hard disk read heads [1,2]. Exchange bias leads to a unidirectional anisotropy, a shift of the hysteresis loop, and often an increase in coercivity [3,4]. Size effects in exchange-biased FM or AFM bilayers have been studied in several systems in which both layers were deposited sequentially then patterned to have the same lateral dimensions [5–9]. For example, in bilayer FM and AFM stripes consisting of ferromagnetic metals coupled to CoO, NiO, FeMn, or IrMn antiferromagnetic layers, exchange bias along the stripe axis decreased as the stripe width decreased [6,7,10,11], but in another example of NiFe/NiO stripes, the exchange bias increased with decreasing stripe width [12].

The magnetic behavior of locally-exchange-biased thin films in which the FM and AFM have different dimensions and the exchange bias is limited to only part of the FM, differs qualitatively from that of patterned FM or AF bilayers. The reversal mechanism of the FM depends on the length scales of the pinned and unpinned regions and the strength of the exchange bias in the pinned regions. Locally-exchange-biased structures are not only essential for certain domain-wall memory or logic devices [10,13] but also provide insights into exchange-bias phenomena [14,15]. For example, continuous NiFe films with overlaid FeMn stripes of micrometer-scale period showed asymmetrical hysteresis loops [16,17] suggesting the pinned and unpinned regions reverse at different fields. Exchange bias parallel to the stripes produced switching in two steps, whereas exchange bias perpendicular to the stripes produced switching in one step [18]. Understanding and manipulating the reversal process of a magnetic film with local exchange bias is, therefore, a key part of magnetic device design, providing, for example, the ability to trap a domain wall or to initiate reversal in a magnetic nanostructure. However, despite its importance, the behavior of magnetic films patterned with submicron antiferromagnetic features and how the regions interact at smaller dimensions has not been explored.

This study analyzes the switching behavior of NiFe continuous films patterned with stripes of IrMn as a function of both the period and width of the IrMn stripes. The structures are made by a two-step deposition process and subsequently field cooled. Phase maps describe the reversal process as a function of pattern geometry, and the results are compared to micromagnetic predictions. The results show the interplay between interface exchange bias and the exchange coupling within the bulk of the NiFe film in determining the hysteresis behavior.

Magnetic films with local exchange bias can be prepared subtractively, i.e. the removal of regions of the AF from an AF or FM bilayer. This can be accomplished by ion-beam etching [16], but this is a nonselective etch which can also damage the FM [19]. Ion bombardment of an AF or FM bilayer through a resist mask can locally alter magnetic properties [14,15,17], for example, by oxidizing an AFM in select portions of the film [18]. However, the lateral resolution of this technique is limited by ion straggle, and it has been limited to introducing exchange bias into features larger than 1 μm. Alternatively, additive methods have been developed, such as the deposition of FM nanodots onto a continuous AFM layer through a porous membrane used as a shadow mask [7]. However, contamination of the AF or FM interface between the two separate deposition steps can degrade the exchange bias. To improve the interface coupling, we previously presented a hybrid

*caross@mit.edu

method [20] in which a predeposited NiFe film was etched back by 1 nm to remove any surface oxides, followed by growth of 1 nm additional NiFe then an IrMn film. This produced exchange bias similar to that found in NiFe/IrMn grown without a vacuum break.

II. METHODS

The patterned samples are prepared using a modification of a process presented earlier [20]. Ta (5 nm)/$Ni_{80}Fe_{20}$ (10 nm) is deposited on top of a Si wafer using triode sputtering at 2×10^{-8} Torr base pressure and 1 m Torr Ar pressure with a growth rate of 0.132 nm s^{-1}. A grating pattern mask is then fabricated on the NiFe using interference lithography [21]. A trilayer stack of antireflective coating (ARC) (315 nm)/SiO_2 (20 nm)/PS4 negative resist (Ohka) (215 nm) is first deposited, as shown in the schematic in Fig. 1. The thickness of the ARC is chosen to minimize reflections of the laser from the substrate to prevent vertical standing waves. The ARC layer is made by spin coating and baking, then the silica layer by electron-beam evaporation, and a thin layer of hexamethyldisilazane is spun to promote adhesion of the PS4 resist onto the silica. The PS4 resist is spun at 3 krpm and baked at 90 °C for 90 s. The resist is then exposed to two beams from a 325-nm wavelength HeCd laser source whose interference produces a grating pattern exposure with periodicity of 240 nm to 1 μm. The resist is then developed, and a two-step RIE process is performed to transfer the pattern into the ARC: CF_4 to etch the SiO_2 and then O_2 to etch the ARC to form a grating. Figure 1(b) shows a scanning electron microscope (SEM) image of the resulting mask.

The samples are then ion-beam etched for 3 s (Ar pressure 2×10^{-4} Torr, beam current 5.5 mA, voltage 500 V, etch rate 0.256 nm s^{-1}) to clean the exposed surface of the NiFe. A 1-nm layer of NiFe is then deposited followed by IrMn (10 nm) deposited at 1 m Torr Ar pressure at a rate of 0.2 nm s^{-1}, then a layer of Ta (5 nm) to prevent oxidation of the magnetic layers. Last, the remaining ARC stack is lifted off using N-methyl-2-pyrrolidone. A SEM image of the final structure is shown in Fig. 1(c). This procedure results in a film of NiFe exchange coupled to overlaid stripes of IrMn. The IrMn stripe periodicity varies from 240 nm to 1 μm while the stripe width varies from 100 to 500 nm. Unpatterned control samples of IrMn/NiFe are also made for comparison. The interference lithography process produces samples of area 5×5 mm^2 with large enough magnetic moment to be measurable using vibrating sample magnetometry (ADE model 1660) at room temperature.

To exclude effects from the ion-beam etch on the magnetic properties of the NiFe, the hysteresis loop of an as-grown 10-nm NiFe film is compared with a 10-nm NiFe film that is subjected to 3 s of ion-beam etching, followed by redeposition of 1-nm NiFe. The loops are measured up to 1000 Oe, with increments of 1 Oe near the switching field. The films have the same coercivity, switching field, and magnetization to within the resolution of the measurement.

The exchange bias is initially set by field cooling at 10 kOe from a temperature of 520 K. The exchange bias is set either parallel to the IrMn stripes or in plane perpendicular to the IrMn stripes. Because of significant training effects [22] as seen in NiFe/IrMn dots [20], the samples are field cooled from 550 K after each hysteresis measurement.

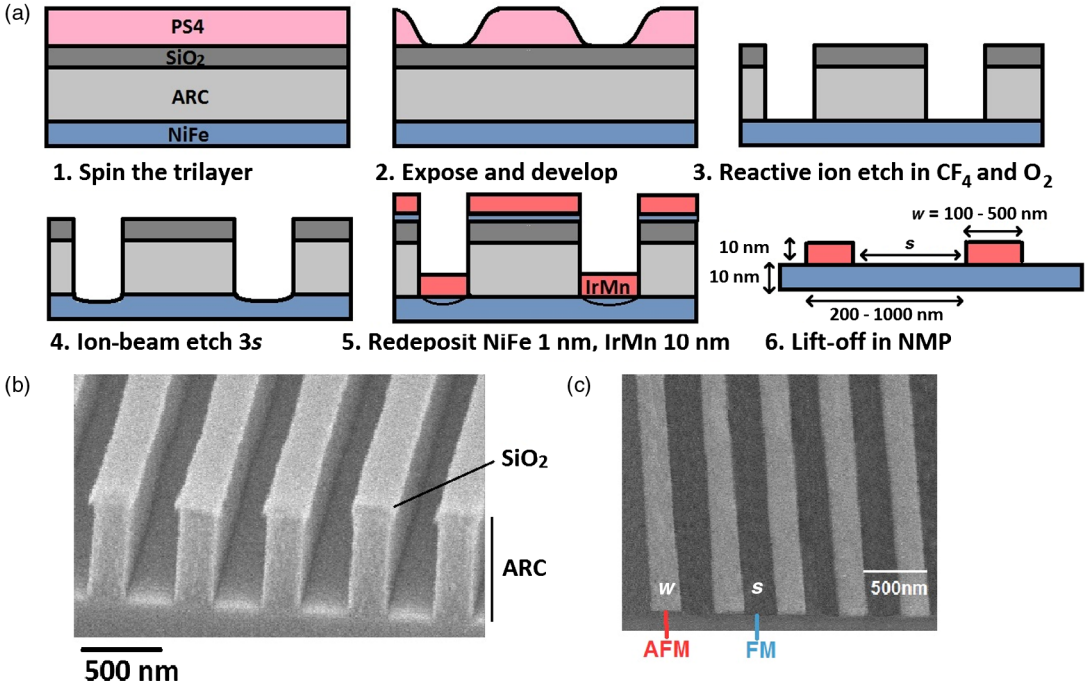

FIG. 1. (a) Schematic of the sample fabrication procedure. In steps 1–3 the resist mask is made; in steps 4–6 the AFM is patterned. (b) SEM image of a resist mask with period 500 nm. (c) SEM image of a patterned sample with period 500 nm showing IrMn stripes of width w separated by regions of unbiased NiFe of width s.

The Object Oriented MicroMagnetic Framework (OOMMF) package [23] is used to model the switching behavior as a function of the IrMn stripe width and spacing. The OOMMF time driver is based on the Landau-Lifshitz-Gilbert equation [24], $dM/dt = -\gamma[M \times H_{\text{eff}}] - \alpha(M/M_s) \times (dM/dt)$, where γ is the electron gyromagnetic ratio, M is the magnetization, H_{eff} is the effective field which includes the external magnetic field and the demagnetizing field, and α is the damping factor. A damping factor of 0.5 is used in these simulations for fast convergence. A saturation magnetization of 800 emu cm^{-3}, exchange stiffness of 1.3×10^{-6} erg cm^{-1}, and an anisotropy energy of 8000 erg cm^{-3} are used [23]. The cell size is 5 $\times$ 5 $\times$ 5 nm^3, as used in prior simulations of NiFe [23] and consistent with the exchange length of NiFe (approximately 5.7 nm) [25]. The simulation size in the direction parallel to the stripes is 2 μm to minimize the influence of edge effects. The exchange bias is modeled as a fixed external field present in the regions of NiFe covered with the IrMn stripes. This is a simplification of the exchange bias, which affects only the NiFe at the NiFe/IrMn interface, but it is justified here because the film thickness corresponds to only two layers of cells which have almost identical magnetization directions. Periodic boundary conditions in the in-plane direction perpendicular to the stripes are used to model an infinite stripe array.

III. RESULTS AND DISCUSSION

A. Exchange bias parallel to grating

We first discuss in Fig. 2 the experimental results for samples with exchange bias and applied field parallel to the stripes, with s (the width of the unbiased regions of NiFe) and w (the width of the biased regions of NiFe) in the range of 100 to 500 nm. At small w and s, the hysteresis loops show a single step [Fig. 2(b)], but as the dimensions increase, the loops show two steps attributed to the switching of the pinned and unpinned regions of the film [Figs. 2(c)–(e)]. The criterion to identify a two-step reversal is the existence of a kink or plateau on at least one branch of the hysteresis loop occurring at a magnetic moment close to the value expected from the relative widths w and s of the stripes. In some cases, the plateau is only evident on one branch of the hysteresis loop, as in Fig. 2(c), because on the other branch, the offset of the loop due to exchange bias is counteracted by an increase in coercivity.

The type of hysteresis loop of all the samples is plotted on a phase diagram, Fig. 2(a), showing a region of one-step reversal for values of w and s below 300 nm; i.e., for these dimensions, the pinned and unpinned regions reverse within a few Oersteds of each other.

In the samples that show two-step reversal, we expect the magnetization at the plateau to be simply related to the ratio of s and w. For example, in Fig. 2(c), the geometry of the sample ($w = 200$ nm, $s = 300$ nm) suggests the first step of

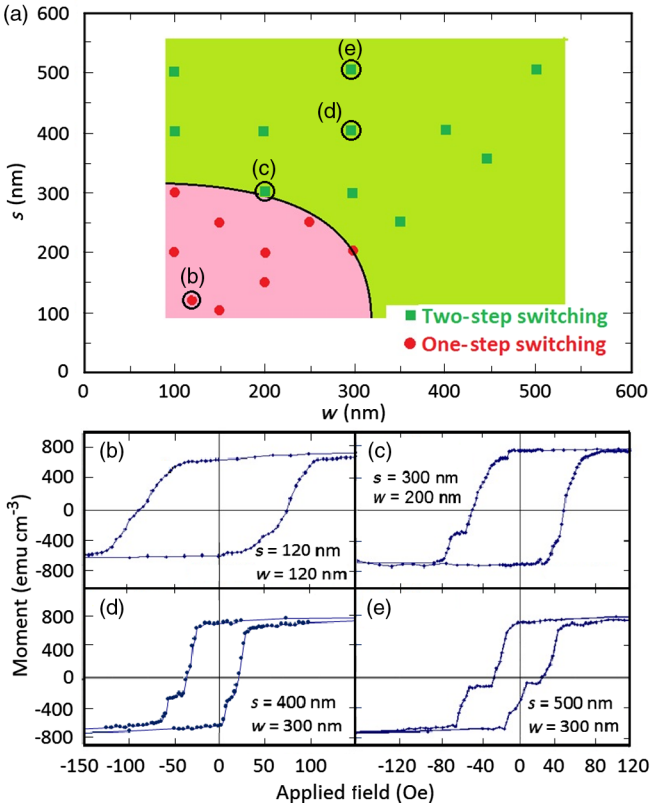

FIG. 2. (a) Experimental phase diagram of the switching behavior. (b) An example of one-step switching, for $s = w = 120$ nm. Example loops for two-step switching: (c) $s = 300$ nm, $w = 200$ nm; (d) $s = 400$ nm, $w = 300$ nm; (e) $s = 500$ nm, $w = 300$ nm.

the descending branch of the hysteresis loop will correspond to 0.6 of the total change in magnetization. However, the measured step height is 0.67; i.e. the effective width of the pinned region is 167 nm. This effective width is consistent with part of the pinned region, in this case 17 nm, reversing with the unpinned region due to exchange coupling in the NiFe film. Samples with other dimensions show similar results with the effective width of the unpinned region given by the nominal width plus 15 nm $\pm$ 2 nm.

Figure 3 shows the trends in coercivity and exchange bias with pattern dimensions. The coercivity of two-step loops is defined as the field at which the unpinned region magnetization reverses, measured halfway up the step. The coercivity increases from 60 to 150 Oe as s decreases, but there is no systematic variation with w. The coercivity of unpatterned NiFe/IrMn samples varies from 100 to 170 Oe.

The exchange bias is 25–70 Oe. As a comparison, unpatterned NiFe/IrMn bilayer films show exchange bias of 80–120 Oe. A reduction of exchange bias in patterned structures compared to continuous bilayers is consistent with other studies [26,27]. The exchange bias increases slowly with s. It shows little variation for 100 nm $\leq w \leq$ 350 nm but is larger for $w = 500$ nm. Prior work [3] shows that a reduction of feature size can cause an increase,

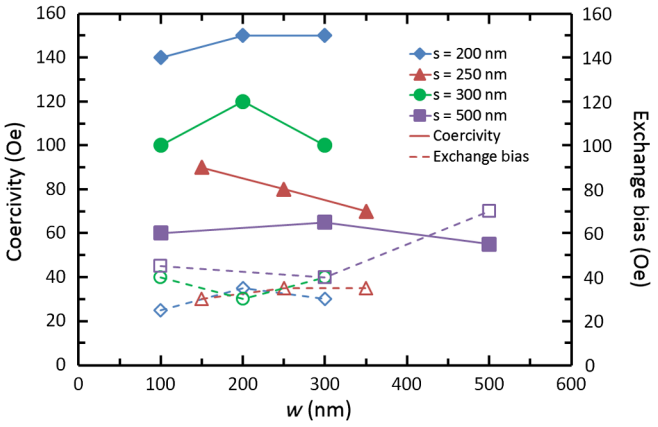

FIG. 3. Measured exchange bias and coercivity versus IrMn stripe width w for four different values of s. For samples that show two-step switching, the coercivity is for the unpinned region.

decrease, or no change in the exchange bias. The magnitude of the exchange bias has been associated with the AFM domain size [27], which is limited by the size of the features in patterned samples. In our system, the 10-nm-thick IrMn is expected to have a domain size of approximately 320 nm [27], wider than the narrowest values of w, suggesting that exchange bias will increase with decreasing w. On the other hand, features with narrower w are more vulnerable to thermal instability of the moments near the edges of the structures [11].

To interpret the results, micromagnetic simulations are performed with the magnetic field and the exchange bias of 100 Oe both parallel to the stripe length y, Fig. 4. The schematic in Fig. 4(a) shows a unit cell used in the simulation. Each data point in the modeled hysteresis loops indicates the magnetization along y calculated after initializing the moments to random directions then allowing them to relax in the corresponding applied field. This method is used to produce ground-state magnetization configurations as a function of field. Calculations in which the magnetic configuration is allowed to evolve as a function of field without reinitializing at each field step lead to very high switching fields due to the high symmetry and the periodic boundary conditions, trapping metastable configurations. This behavior is the case even when notches, a field offset of 2°, or a spread in magnetic anisotropy between cells is introduced.

Examples are shown in Figs. 4(b)–4(e) for several combinations of w and s. For smaller dimensions, the magnetization in the relaxed state is aligned along either $+y$ or $-y$ with high remanence [Fig. 4(b)], but for larger dimensions, a limited range of fields produces a state in which the magnetization of the pinned and unpinned regions of the NiFe is antiparallel, and the net magnetization takes an intermediate value [Figs. 4(c)–4(e)]. These cases represent one-step and two-step reversal, respectively. Figure 4(a) shows a phase diagram that summarizes the

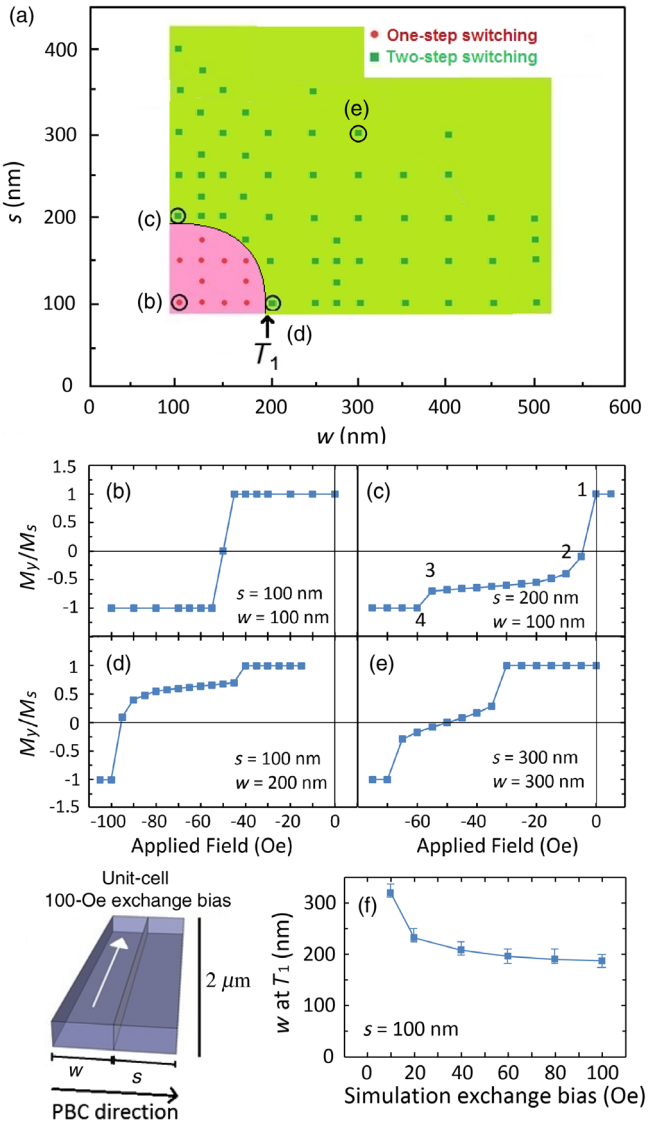

FIG. 4. (a) Phase diagram for switching behavior of the patterned structure with both exchange bias and applied field parallel to the stripe length. T_1 indicates the phase boundary. (b) An example of one-step switching, and [(c)–(e)] examples of two-step switching. The dimensions correspond with the points labeled (b)–(e) in the phase diagram. The numbers in the hysteresis loop (c) refer to the micromagnetic images in Fig. 5. (f) The values of w for $s = 200$ nm at the transition T_1 as a function of exchange bias.

results as a function of s and w. The phase boundary between one-step and two-step reversal is labeled T_1 and resembles the experimental results, Fig. 2(a). For two-step reversal, the value of magnetization at the plateau is field-dependent, showing that the width of the reversed region does not simply correspond to the width of the unpinned region but increases with increasing field.

The reversal process can be seen in more detail from the micromagnetic configurations vs field. Figure 5 shows an example from the descending branch loop of Fig. 4(c)

($w = 100$ nm, $s = 200$ nm) with positive magnetization direction in red and negative in blue. The unpinned region, as well as 14 nm width of the pinned region, reverse in panel 2 at −5 Oe. This distance is about twice the exchange length of NiFe (approximately 5.7 nm) [25]. Similar behavior is seen for other model geometries exhibiting two-step loops. As the reverse field increases to −55 Oe, panel 3, the pinned region gradually reverses from the edges and reduces in width, with reversal completed at −60 Oe, panel 4. In contrast, complementary behavior is seen in simulations with $w > s$ [Fig. 4(d)] ($w = 200$ nm, $s = 100$ nm). At the switching field of −45 Oe, only the center part of the unpinned region switches. Increasing negative fields lead to a gradual expansion of the reversed region and reversal is complete at −100 Oe.

The pinning is simply modeled as a region subject to a different effective field. During the reversal, exchange coupling causes part of the narrower region to switch with the wider region. In the case of $w = s$, increasing the negative field first reverses the center of the unpinned region which expands into the pinned region as the field increases, and the midpoint of the plateau corresponds to zero net magnetization [Figs. 4(b) and 4(e)].

In contrast, for combinations of s and w within boundary T_1, both pinned and unpinned regions reverse together without the formation of 180° walls. As the exchange bias in the model decreases, T_1 moves to larger values of w and s. Figure 4(f) shows the change in T_1 with exchange bias. For example, when $s = 200$ nm, T_1 occurs at $w = 100$ nm for 100-Oe exchange bias and at $w = 150$ nm for 40-Oe exchange bias.

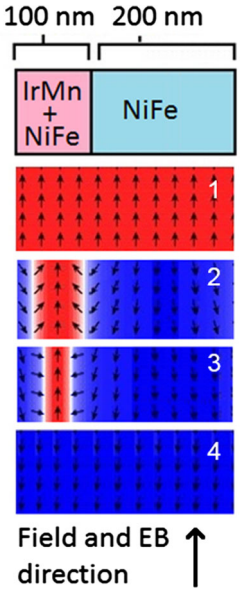

FIG. 5. OOMMF micromagnetic images under fields corresponding to Fig. 3(c), for $s = 200$ nm, $w = 100$ nm. Panels 1, 2, 3, 4 depict the equilibrium configuration at 0, −5, −55, and −60 Oe, respectively.

The model, therefore, shows that one-step switching is promoted at lower stripe dimensions both by the increased energetic cost per unit area of forming the 180° domain walls and by the reduction in exchange bias in structures with lower dimensions. The agreement with the experiment is quite good considering the simplifications of the model, which include zero temperature, periodic boundary conditions in only one direction, and the treatment of exchange bias as a fixed Zeeman field in the film. More realistic treatment of exchange bias, such as modeling the AF as a fraction of pinned and rotatable magnetic cells representing uncompensated moments [28], may produce better quantitative agreement with the experimental observations.

B. Exchange bias perpendicular to grating

When the field cooling and applied field are in plane, perpendicular to the stripe length, two-step switching is observed in samples with larger w and s, summarized in the phase diagram in Fig. 6(a). The boundary T_2 between one-step and two-step switching regimes occurs at higher w and s compared with T_1 described above for samples with exchange bias parallel to the lines. Moreover, the measured exchange bias in the two-step loops is 20 to 35 Oe, lower than for the parallel case (25 to 50 Oe). This result differs from a study of wider stripes [19], which observed no two-step switching, even up to 20-μm periodicity.

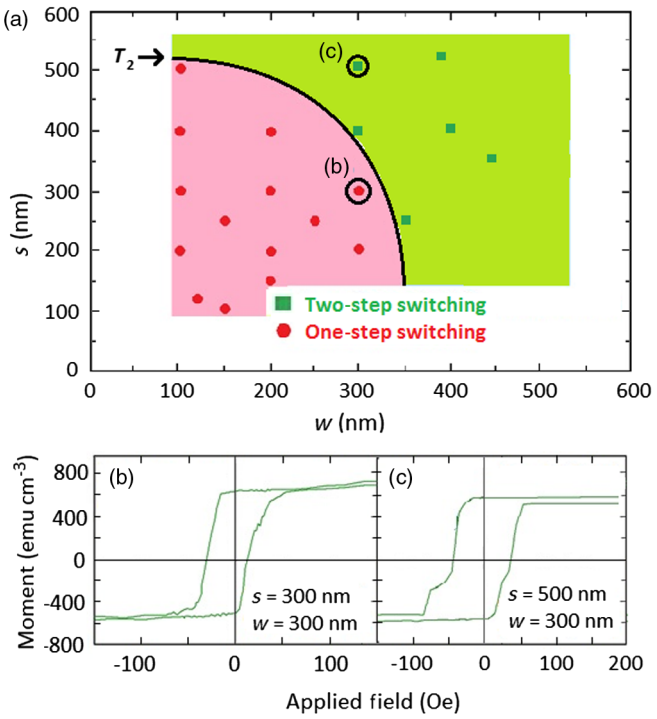

FIG. 6. (a) Experimental phase diagram of the switching behavior in the samples exchange biased and measured perpendicular to the wire length. (b) An example loop for one-step switching. (c) An example loop for two-step switching.

The simulations, however, predict one-step switching for all combinations of w and s tested in the range of 100 to 500 nm [Fig. 7(a)]. This result is obtained for hysteresis loops calculated with no offset or with a 1° offset between the applied field and the direction transverse to the lines in order to break the symmetry of the simulation and also for relaxation from a random magnetization state. Images of the equilibrium magnetic configuration are shown at fields of −170 and −180 Oe, just below and just above the switching field [Figs. 7(c) and 7(d)], as well as a dynamic intermediate state calculated from the state at Fig. 7(c) by applying a field of −180 Oe with damping parameter $\alpha = 0.01$. The switching proceeds incoherently with the unpinned region reversing first, producing a head-to-head 180° domain wall.

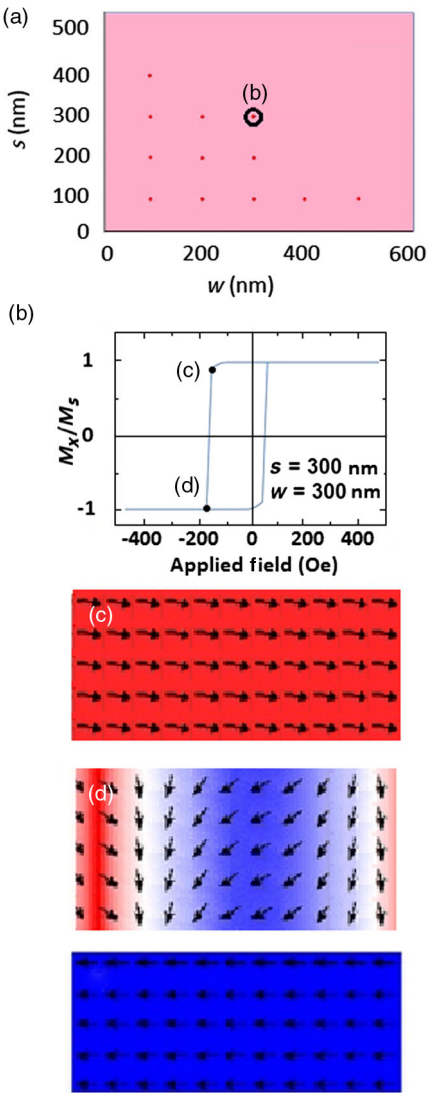

FIG. 7. (a) Phase diagram for switching behavior of the patterned structure with exchange bias in plane along x, perpendicular to the wire length. All the modeled dimensions result in one-step switching. (b) Example of a loop showing one-step switching. Magnetic configurations are shown at 170 Oe before the switch (c), and at 180 Oe after the switch (d), along with an intermediate state calculated dynamically by applying a field of 180 Oe to (c). The figures represent 600 nm width.

A larger simulation with an increased exchange bias of 1000 Oe and $s = w = 2000$ nm produces two-step switching, which shows that for sufficiently large exchange bias and wire widths, two-step switching can take place. However, for the smaller dimensions and lower exchange bias in Fig. 7(a), the energetic cost of the head-to-head 180° domain walls, which have greater stray field and greater width than the walls formed when the exchange bias and field are parallel to the stripes, preclude two-step reversal in the model.

In comparison, 30-nm NiFe patterned with (2–20)-μm IrMn stripes [18] shows only single-step reversal for exchange bias and field perpendicular to the stripes. The lack of two-step switching is attributed to the interstripe extension of domain walls and overlapping tails of the Néel walls. Furthermore, the greater thickness of the NiFe (and, hence, the domain-wall size) and the modest exchange-bias values (a few oersteds) will promote single-step switching behavior at much larger stripe dimensions.

IV. SUMMARY

Local exchange bias is obtained in continuous 10-nm-thick NiFe films overlaid with arrays of 10-nm-thick IrMn stripes. The samples are fabricated using interference lithography combined with an etch and sputter deposition process to yield stripe widths of 100–500 nm and periods of 240–1000 nm. The magnetic switching behavior is mapped out as a function of dimensions both experimentally and by micromagnetic modeling. In the patterned samples, at low wire widths and spacings, the pinned and free regions switch together, but as the width and spacing of the wires increases, the pinned and unpinned regions reverse at different fields giving a two-step loop. Micromagnetic modeling provides insight into the reversal process, reproducing the change in reversal process with stripe width for exchange bias and field parallel to the stripes. However, the simulations predict single-step reversal for exchange bias and field perpendicular to the stripes unless the exchange bias and period are large, which disagrees with the experiments.

Although the fabrication method and magnetic properties are demonstrated for a continuous film of NiFe, these results can be extended to structures in which the FM layer is also patterned, such as magnetic memory devices consisting of magnetic wires with AF pads at the ends [13] or to exchange-biased materials with perpendicular anisotropy. These results demonstrate the effect of pattern dimensions on the magnetic properties and reversal mechanisms of locally-exchange-biased thin films.

ACKNOWLEDGMENTS

The authors gratefully acknowledge the support of the National Science Foundation and C-SPIN, a STARnet Center of the Semiconductor Research Corporation supported by DARPA and MARCO. Facilities of the MIT Center for Materials Science and Engineering (NSF Grant No. DMR1419807) and the NanoStructures Laboratory were used. We thank Jim Daley for his assistance with electron-beam evaporation and Dr. Tim Savas for his advice on interference lithography.

[1] V. Baltz, J. Sort, B. Rodmacq, B. Dieny, and S. Landis, Size effects on exchange bias in sub-100 nm ferromagnetic-antiferromagnetic dots deposited on prepatterned substrates, Appl. Phys. Lett. **84**, 4923 (2004).

[2] A. Hoffmann, M. Grimsditch, J. E. Pearson, J. Nogues, W. A. A. Macedo, and I. K. Schuller, Tailoring the exchange bias via shape anisotropy in ferromagnetic/antiferromagnetic exchange-coupled systems, Phys. Rev. B **67**, 220406 (2003).

[3] J. Nogues, J. Sort, V. Langlais, V. Skumryev, S. Surinach, J. S. Munoz, and M. D. Baro, Exchange bias in nanostructures, Phys. Rep. **422**, 65 (2005).

[4] J. Nogues and I. K. Schuller, Exchange bias, J. Magn. Magn. Mater. **192**, 203 (1999).

[5] Z. P. Li, O. Petracic, J. Eisenmenger, and I. K. Schuller, Reversal behavior of exchange-biased submicron dots, Appl. Phys. Lett. **86**, 072501 (2005).

[6] Y. Shen, Y. Wu, H. Xie, K. Li, J. Qiu, and Z. Guo, Exchange bias of patterned NiFe/IrMn film, J. Appl. Phys. **91**, 8001 (2002).

[7] K. Liu, J. Nogues, C. Leighton, H. Masuda, K. Nishio, I. V. Roshchin, and I. K. Schuller, Fabrication and thermal stability of arrays of Fe nanodots, Appl. Phys. Lett. **81**, 4434 (2002).

[8] J. Yu, A. D. Kent, and S. S. P. Parkin, Exchange biasing in polycrystalline thin film microstructures, J. Appl. Phys. **87**, 5049 (2000).

[9] E. Girgis, R. D. Portugal, M. J. Van Bael, K. Temst, and C. Van, Haesendonck, Asymmetric magnetization reversal in exchange-biased NiFe/CoO submicron-sized structures, J. Appl. Phys. **97**, 103911 (2005).

[10] D. M. Bromberg, D. H. Morris, L. Pileggi, and J. Zhu, Novel STT-MTJ device enabling all-metallic logic circuits, IEEE Trans. Magn. **48**, 3215 (2012).

[11] M. Fraune, U. Rudiger, G. Guntherodt, C. Cardoso, and P. Freitas, Size dependence of the exchange bias field in NiO/Ni nanostructures, Appl. Phys. Lett. **77**, 3815 (2000).

[12] A. Nemoto, Y. Otani, S. G. Kim, K. Fukamichi, O. Kitakami, and Y. Shimada, Magnetoresistance and planar Hall effects in submicron exchange-coupled $NiO/Fe_{19}Ni_{81}$ wires, Appl. Phys. Lett. **74**, 4026 (1999).

[13] J. A. Currivan, Y. Jang, M. D. Mascaro, M. A. Baldo, and C. A. Ross, Low energy magnetic domain wall logic in short, narrow, ferromagnetic wires, IEEE Magn. Lett. **3**, 3000104 (2012).

[14] J. Fassbender and J. McCord, Magnetic patterning by means of ion irradiation and implantation, J. Magn. Magn. Mater. **320**, 579 (2008).

[15] J. McCord, L. Schultz, and J. Fassbender, Hybrid soft-magnetic lateral exchange spring films prepared by ion irradiation, Adv. Mater. **20**, 2090 (2008).

[16] Z. B. Guo, K. B. Li, G. C. Han, Z. Y. Liu, P. Luo, and Y. H. Wu, Exchange bias in patterned FeMn/NiFe bilayers, J. Magn. Magn. Mater. **251**, 323 (2002).

[17] C. Hamann, J. McCord, L. Schultz, B. P. Toperverg, K. Theis-Bröhl, M. Wolff, R. Kaltofen, and I. Mönch, Competing magnetic interactions in exchange-bias-modulated films, Phys. Rev. B **81**, 024420 (2010).

[18] C. Hamann, I. Monch, R. Kaltofen, R. Schafer, T. Gemming, L. Schultz, and J. McCord, Size effects on the magnetization reversal behavior of exchange bias modulated thin films, J. Appl. Phys. **104**, 013926 (2008).

[19] A. Scherer, H. G. Craighead, M. L. Roukes, and J. P. Harbison, Electrical damage induced by ion beam etching of GaAs, J. Vac. Sci. Technol. B **6**, 277 (1988).

[20] F. Liu and C. A. Ross, Size-dependent magnetic properties of 100–500 nm diameter IrMn/NiFe disks made by a two-step deposition process, J. Appl. Phys. **116**, 194307 (2014).

[21] A. Gombert, B. Bläsi, Ch. Bühler, P. Nitz, J. Mick, W. Hoßfeld, and M. Niggemann, Some application cases and related manufacturing techniques for optically functional microstructures on large areas, Opt. Eng. **43**, 2525 (2004).

[22] C. Binek, S. Polisetty, X. He, and A. Berger, Exchange Bias Training Effect in Coupled All Ferromagnetic Bilayer Structures, Phys. Rev. Lett. **96**, 067201 (2006).

[23] M. Donahue and D. Porter, http://math. nist. gov/oommf.

[24] T. L. Gilbert, A phenomenological theory of damping in ferromagnetic materials, IEEE Trans. Magn. **40**, 3443 (2004).

[25] G. S. Abo, Y. Hong, J. Park, J. Lee, W. Lee, and B. Choi, Definition of magnetic exchange length, IEEE Trans. Magn. **49**, 4937 (2013).

[26] J. I. Martin, J. Nogués, K. Liu, J. L. Vicent, and I. K. Schuller, Ordered magnetic nanostructures: fabrication and properties, J. Magn. Magn. Mater. **256**, 449 (2003).

[27] V. Baltz, J. Sort, S. Landis, B. Rodmacq, and B. Dieny, Tailoring Size Effects on the Exchange Bias in Ferromagnetic-Antiferromagnetic <100 nm Nanostructures, Phys. Rev. Lett. **94**, 117201 (2005).

[28] D. A. Gilbert, L. Ye, A. Varea, S. Agramunt-Puig, N. del Valle, C. Navau, J. F. López-Barbera, K. S. Buchanan, A. Hoffmann, A. Sánchez, J. Sort, K. Liu,, and J. Nogués, A new reversal mode in exchange coupled antiferromagnetic/ferromagnetic disks: Distorted viscous vortex, Nanoscale **7**, 9878 (2015).